Surface Science Spectra

RESEARCH ARTICLE | NOVEMBER 11 2024

XPS investigation of Cu_xO-functionalized amorphous carbon nitride

Special Collection: Materials for Energy and the Environment

Giacomo Marchiori ; Mattia Benedet ; Angelica Fasan ; Davide Barreca ; Chiara Maccato ; Gian Andrea Rizzi ; Alberto Gasparotto

Surf. Sci. Spectra 31, 024010 (2024)
https://doi.org/10.1116/6.0004078

SSS SURFACE SCIENCE SPECTRA ARTICLE pubs.aip.org/avs/sss

XPS investigation of Cu_xO-functionalized amorphous carbon nitride

Cite as: Surf. Sci. Spectra **31**, 024010 (2024); doi: 10.1116/6.0004078
Submitted: 16 September 2024 · Accepted: 25 October 2024 ·
Published Online: 11 November 2024

View Online Export Citation CrossMark

Giacomo Marchiori,[1] Mattia Benedet,[1,2] Angelica Fasan,[2] Davide Barreca,[2,a)] Chiara Maccato,[1,2] Gian Andrea Rizzi,[1,2] and Alberto Gasparotto[1,2]

AFFILIATIONS

[1]Department of Chemical Sciences, Padova University and INSTM, 35131 Padova, Italy
[2]CNR-ICMATE and INSTM, Department of Chemical Sciences, Padova University, 35131 Padova, Italy

Note: This paper is part of the 2024 Special Topic Collection on Materials for Energy and the Environment.
[a)]**Author to whom correspondence should be addressed:** davide.barreca@unipd.it

ABSTRACT

In this work, we report the x-ray photoelectron spectroscopy characterization of a novel nanocomposite (photo)electrocatalyst for the oxygen evolution reaction, based on amorphous carbon nitride (aCN) functionalized with Cu_xO nanoparticles (NPs). The specimen has been fabricated employing two sequential plasma-assisted processes, involving the initial aCN deposition onto conductive glass *via* magnetron sputtering, followed by carbon nitride functionalization with Cu_xO (x = 1, 2) NPs by radio frequency-sputtering. The results reported herein include the survey spectrum and the high-resolution C 1*s*, N 1*s*, O 1*s*, Cu 2*p*, and Cu *LMM* signals. The most significant spectral features are analyzed and critically discussed.

Accession #: 01978
Technique: XPS and XAES
Specimen: aCN-Cu_xO
Instrument: ThermoFisher Scientific EscalabTM QXi
Major Elements in Spectra: C, N, O, and Cu
Minor Elements in Spectra: None
Published Spectra: 6
Spectral Category: Comparison

INTRODUCTION

The development of efficient and clean energy production and conversion technologies represents an open challenge of utmost importance for sustainable development (Refs. 1–4). In this context, (photo)electrochemical water splitting yielding green H_2 is regarded as the "holy grail" of the future energy infrastructure (Refs. 5–7). However, the overall process is strongly limited by the oxygen evolution reaction (OER) that, due to its high overpotential and intrinsic kinetic limitations, severely hampers H_2 generation yield (Refs. 3, 8, and 9).

In the present work, we report on the synthesis and characterization of a novel nanocomposite material, specifically designed to be employed as OER (photo)electrocatalyst. The specimen was prepared by a two-step, low-temperature plasma-assisted route, which has never been adopted so far for the fabrication of analogous systems. First, amorphous carbon nitride (aCN) was deposited onto conductive fluorine-doped tin oxide (FTO) *via* reactive magnetron sputtering, using a graphite target in Ar/N_2 atmosphere. Subsequently, highly dispersed copper oxide (Cu_xO, x = 1, 2) nanoparticles (NPs) were grown on top of the aCN deposit by means of RF-sputtering. Amorphous carbon nitride systems, characterized by an N/C atomic ratio lower than stoichiometric C_3N_4 (Refs. 10 and 11), display a remarkable chemical stability and favorable physical and mechanical features, thanks to their covalently bonded network (Refs. 12 and 13). Whereas some papers have reported on the use of powdered aCN for photocatalytic evolution of H_2 (Refs. 14–16), the investigation of the material as supported OER (photo)electrocatalyst is still in its preliminary stages, particularly if compared to crystalline graphitic carbon nitride (g-C_3N_4) (Refs. 15 and 17). On the other hand, nanostructured copper

oxides (Cu_2O and CuO, both *p*-type semiconductors with a band gap of ≈2.0 and 1.2/1.5 eV, respectively) have already been extensively studied for (photo)electrocatalytic applications due to their large availability, low cost, nontoxicity, and significant vis-light absorption (Refs. 5 and 18). In a different way, the synthesis and characterization of aCN-Cu_xO nanocomposites undoubtedly deserves further attention for both fundamental and applicative purposes.

In this work, the use of plasma sputtering for the synthesis of the composite material allowed to achieve an intimate contact between aCN and Cu_xO. This feature results in the formation of heterojunctions between *p*-type copper oxides and *n*-type carbon nitride, improving charge separation and boosting catalytic activity toward OER under illumination (Refs. 2, 3, 19, and 20). In addition, the carbon nitride matrix also promoted the ultradispersion of copper oxides NPs, stabilizing them against aggregation (Refs. 9 and 21).

In the following, a detailed XPS investigation of a representative aCN-Cu_xO sample is reported, focusing on the analysis of C 1*s*, N 1*s*, O 1*s*, Cu 2*p*, and Cu *LMM* spectral regions, providing information on the elemental chemical states. The collected data, unavailable in the literature up to date, could be useful to researchers focusing on the XPS investigation of amorphous carbon nitride-based nanomaterials.

SPECIMEN DESCRIPTION (ACCESSION # 01978)

Specimen: aCN-Cu_xO
CAS Registry #: Unknown
Specimen Characteristics: Homogeneous; solid; amorphous; semiconductor; composite
Chemical Name: Amorphous carbon nitride-copper (I)/copper (II) oxides
Source: Sample prepared by aCN magnetron sputtering deposition on FTO and subsequent annealing in Ar at 500 °C for 2.5 h, followed by functionalization with Cu_xO NPs by RF-sputtering for 15 min and final thermal treatment in Ar at 450 °C for 2.5 h.
Composition: C, N, O, and Cu
Form: Supported nanocomposite
Structure: X-ray diffraction (XRD) analyses only revealed reflections from the FTO substrate, whereas no signals originating from the aCN-Cu_xO deposit were detected. Such a result was traced back to the amorphous nature of the carbon nitride layer and to the low amount and high dispersion of copper oxide NPs. Fourier-transform infrared (FT-IR) spectroscopy measurements showed a broad band in the 1100–1700 cm^{-1} region, associated to characteristic vibrational modes of the nitride network (Refs. 22 and 23). Moreover, a small but well distinguishable peak at ≈2220 cm^{-1} was observed, pointing out to the presence of —C≡N groups (Ref. 24). The broad and multicomponent band between 2600 and 3600 cm^{-1} was associated to the stretching modes of chemisorbed O—H moieties, as well as to C—H and N—H terminal groups (Ref. 8). Scanning electron microscopy (SEM) evidenced that the aCN deposit consisted of a relatively compact and well-adherent film with a thickness of ≈450 nm. Transmission electron microscopy (TEM) revealed an ultradispersion of low-sized Cu-containing NPs over the aCN matrix.
History and Significance: The aCN film was synthesized in a custom built multiple-electrode magnetron sputtering apparatus, equipped with a 13.56 MHz RF power source. A pyrolytic graphite target (Nanovision Srl, thickness = 3 mm, diameter = 50 mm, and purity = 99.999%) was fixed to the magnetron source, while a precleaned FTO substrate (2×1 cm^2; Aldrich®; ≈7 $\Omega \times sq^{-1}$; thickness = 600 nm) was mounted on the ground electrode. The synthesis procedure was performed at room temperature under the following conditions: RF power = 100 W; duration = 30 min; total pressure = 5.6×10^{-3} mbar; Ar flow rate = 21 standard cubic centimeters per minute (SCCM); and N_2 flow rate = 42 SCCM. After deposition, the specimen underwent a thermal annealing at 500 °C for 2.5 h in Ar atmosphere. Functionalization with copper oxides was performed by RF-sputtering using a different custom built two-electrode apparatus (ν = 13.56 MHz). A copper target (Alfa Aesar®; thickness = 0.3 mm; and purity = 99.95%) was fixed on the RF electrode, whereas the FTO-supported aCN deposit was mounted on the grounded one. NPs deposition was carried out using the following settings: Ar flow rate = 10 SCCM; total pressure = 0.30 mbar; growth temperature = 60 °C; RF power = 10 W; duration = 15 min; and target-to-substrate distance = 60 mm. Lastly, the material was subjected to a final thermal treatment at 450 °C for 2.5 h in Ar atmosphere.
As-Received Condition: As grown.
Analyzed Region: Same as host material.
***Ex Situ* Preparation/Mounting:** The specimen was mounted on a grounded sample holder by metallic clips and introduced into the chamber through a fast entry system.
***In Situ* Preparation:** The specimen was analyzed as-received.
Charge Control: None
Temp. During Analysis: 298 K
Pressure During Analysis: $<10^{-8}$ Pa
Preanalysis Beam Exposure: 130 s

INSTRUMENT DESCRIPTION

Manufacturer and Model: ThermoFisher Scientific EscalabTM QXi
Analyzer Type: Spherical sector
Detector: Channeltron
Number of Detector Elements: 6

INSTRUMENT PARAMETERS COMMON TO ALL SPECTRA

Analyzer Mode: Constant pass energy
Throughput ($T = E^N$): Calculated from a cubic polynomial fit to a plot of log[peak area/(PE × RSF)] (y) vs log(KE/PE) (x): $y = a + bx + cx^2 + dx^3$, where PE and KE are the pass energy and the kinetic energy, and RSF is the relative sensitivity factor. The coefficients corresponding to the adopted operating conditions are $a = 3.867\,64$; $b = -0.075\,012\,2$; $c = 0.003\,690\,77$; and $d = -0.045\,752\,4$.
Excitation Source Window: None
Excitation Source: Al K_α monochromatic
Source Energy: 1486.6 eV
Source Strength: 200 W

Source Beam Size: $500 \times 500\,\mu m^2$
Signal Mode: Single channel direct

Geometry

Incident Angle: 58°
Source-to-Analyzer Angle: 58°
Emission Angle: 0°
Specimen Azimuthal Angle: 90°
Acceptance Angle from Analyzer Axis: 45°
Analyzer Angular Acceptance Width: 22.5° × 22.5°

Ion Gun

Manufacturer and Model: ThermoFisher Scientific MAGCIS Dual Beam Ion Source
Energy: 4000 eV
Current: 7 mA
Current Measurement Method: Biased stage
Sputtering Species and Charge: Ar^+
Spot Size (unrastered): 500 μm
Raster Size: $4500 \times 4500\,\mu m^2$
Incident Angle: 40°
Polar Angle: 40°
Azimuthal Angle: 270°
Comment: Differentially pumped ion gun

DATA ANALYSIS METHOD

Energy Scale Correction: None.
The analyzer calibration procedure performed in this work was the one proposed by Seah (Ref. 25).
Recommended Energy Scale Shift: 0 eV
Peak Shape and Background Method: In the present work, peak analysis was performed employing the XPSpeak software (version 4.1) (Ref. 26). A Shirley-type background was used. Fitting of C 1*s*, N 1*s*, and O 1*s* peaks was carried out with least-squares fitting method (Ref. 27), adopting Gaussian/Lorentzian sum functions (typical mixing parameter = 0.2–0.3) (Ref. 28) and a number of average points at endpoints equal to 7. No constraints were imposed.
Recommended background start and end points (±0.4 eV) are given below:
C 1*s*: 280–296 eV
N 1*s*: 395–407 eV
O 1*s*: 527–537.5 eV
Quantitation Method: Quantification was accomplished using Thermo Scientific Avantage software (version 6.6.0, Build 00114) by normalizing peak areas for the respective sensitivity factors (Ref. 29). The used sensitivity factors were provided by the same software (peak library: ALTHERMO1; energy correction: TPP-2M IMFF).

ACKNOWLEDGMENTS

This work was financially supported by CNR (Progetti di Ricerca @CNR—avviso 2020—ASSIST), Padova University (P-DiSC#04BIRD2020-UNIPD EUREKA, P-DiSC#02BIRD2023-UNIPD RIGENERA, DOR 2021–2023), INSTM Consortium (INSTM21PDGASPAROTTO-NANOMAT and INSTM21PD BARMAC-ATENA), and PRIN 2022474YE8 SCI-TROPHY project (financed by the European Union—Next Generation EU—Bando PRIN 2022—M4.C2.1.1). The instrumental apparatus used in this work was funded by "Sviluppo delle infrastrutture e programma biennale degli interventi del Consiglio Nazionale delle Ricerche (2019)." Thanks are due to Dr. S. M. Deambrosis, Dr. V. Zin, and Dr. F. Montagner (CNR-ICMATE, Padova, Italy) for valuable support and discussions.

AUTHOR DECLARATIONS

Conflict of Interest

The authors have no conflicts to disclose.

Author Contributions

Giacomo Marchiori: Software (equal); Validation (equal); Visualization (lead); Writing – original draft (lead). **Mattia Benedet:** Data curation (equal); Methodology (equal); Validation (equal); Visualization (equal). **Angelica Fasan:** Investigation (lead); Software (equal); Writing – original draft (equal). **Davide Barreca:** Conceptualization (equal); Formal analysis (equal); Funding acquisition (lead); Supervision (equal); Writing – review & editing (equal). **Chiara Maccato:** Formal analysis (equal); Funding acquisition (equal); Methodology (equal); Supervision (equal); Visualization (equal); Writing – review & editing (equal). **Gian Andrea Rizzi:** Funding acquisition (equal); Visualization (equal); Writing – review & editing (equal). **Alberto Gasparotto:** Data curation (lead); Formal analysis (lead); Funding acquisition (equal); Investigation (lead); Methodology (equal); Writing – review & editing (lead).

DATA AVAILABILITY

The data that support the findings of this study are available within the article and its supplementary material.

REFERENCES

[1] X. Zou, R. Silva, A. Goswami, and T. Asefa, Appl. Surf. Sci. **357**, 221 (2015).
[2] S. M. Hosseini H., R. Siavash Moakhar, F. Soleimani, S. K. Sadrnezhaad, S. Masudy-Panah, R. Katal, A. Seza, N. Ghane, and S. Ramakrishna, Appl. Surf. Sci. **530**, 147271 (2020).
[3] X. Liu, Y. Han, Y. Guo, X. Zhao, D. Pan, K. Li, and Z. Wen, Adv. Energy Sustainability Res. **3**, 2200005 (2022).
[4] H.-Y. Chang and K.-Y. Lee, Jpn. J. Appl. Phys. **54**, 085801 (2015).
[5] H. Bae, V. Burungale, W. Na, H. Rho, S. H. Kang, S. W. Ryu, and J. S. Ha, RSC Adv. **11**, 16083 (2021).
[6] A. M. Paul *et al.*, Diam. Relat. Mater. **107**, 107899 (2020).
[7] S. Zhang, J. Yan, S. Yang, Y. Xu, X. Cai, X. Li, X. Zhang, F. Peng, and Y. Fang, Chin. J. Catal. **38**, 365 (2017).
[8] M. Benedet *et al.*, ACS Appl. Mater. Interfaces **15**, 47368 (2023).
[9] M. Benedet, G. A. Rizzi, A. Gasparotto, O. I. Lebedev, L. Girardi, C. Maccato, and D. Barreca, Chem. Eng. J. **448**, 137645 (2022).
[10] A. G. Fitzgerald, L. Jiang, M. J. Rose, and T. J. Dines, Appl. Surf. Sci. **175–176**, 525 (2001).
[11] N. Hellgren, R. T. Haasch, S. Schmidt, L. Hultman, and I. Petrov, Carbon **108**, 242 (2016).
[12] L. Galán, I. Montero, and F. Rueda, Surf. Coat. Technol. **83**, 103 (1996).

[13]C. Wu, G. Li, X. Cao, B. Lei, and X. Gao, Green Energy Environ. **2**, 302 (2017).
[14]Y. Kang, Y. Yang, L.-C. Yin, X. Kang, G. Liu, and H.-M. Cheng, Adv. Mater. **27**, 4572 (2015).
[15]F. K. Kessler, Y. Zheng, D. Schwarz, C. Merschjann, W. Schnick, X. Wang, and M. J. Bojdys, Nat. Rev. Mater. **2**, 17030 (2017).
[16]B. Yan, Z. Chen, and Y. Xu, Chem. Asian J. **15**, 2329 (2020).
[17]J. Wen, J. Xie, X. Chen, and X. Li, Appl. Surf. Sci. **391**, 72 (2017).
[18]Y. Tian, B. Chang, J. Fu, B. Zhou, J. Liu, F. Xi, and X. Dong, J. Solid State Chem. **212**, 1 (2014).
[19]J. Chen, S. Shen, P. Guo, M. Wang, P. Wu, X. Wang, and L. Guo, Appl. Catal. B **152–153**, 335 (2014).
[20]M. Ismael, J. Alloys Compd. **846**, 156446 (2020).
[21]M. Benedet, G. A. Rizzi, A. Gasparotto, N. Gauquelin, A. Orekhov, J. Verbeeck, C. Maccato, and D. Barreca, Appl. Surf. Sci. **618**, 156652 (2023).
[22]W. Zhang, Q. Zhang, F. Dong, and Z. Zhao, Int. J. Photoenergy **2013**, 685038 (2013).
[23]Y. Zheng, Z. Zhang, and C. Li, J. Photochem. Photobiol. A Chem. **332**, 32 (2017).
[24]F. Li, X. Yue, H. Zhou, J. Fan, and Q. Xiang, Chin. J. Catal. **42**, 1608 (2021).
[25]M. P. Seah, Surf. Interface Anal. **31**, 721 (2001).
[26]See https://xpspeak.software.informer.com/4.1/ for information about the XPS peak fitting program.
[27]D. A. Shirley, Phys. Rev. B **5**, 4709 (1972).
[28]V. Jain, M. C. Biesinger, and M. R. Linford, Appl. Surf. Sci. **447**, 548 (2018).
[29]K. Berresheim, M. Mattern-Klosson, and M. Wilmers, Fresenius J. Anal. Chem. **341**, 121 (1991).
[30]I. Bertóti, M. Mohai, and K. László, Carbon **84**, 185 (2015).
[31]C. Zhang, L. Fu, N. Liu, M. Liu, Y. Wang, and Z. Liu, Adv. Mater. **23**, 1020 (2011).
[32]Y.-C. Lin, C.-Y. Lin, and P.-W. Chiu, Appl. Phys. Lett. **96**, 133110 (2010).
[33]J. F. Moulder, W. F. Stickle, P. E. Sobol, and K. D. Bomben, *Handbook of X-ray Photoelectron Spectroscopy* (Perkin-Elmer Corporation, Eden Prairie, MN, 1992).
[34]D. Barreca, A. Gasparotto, and E. Tondello, Surf. Sci. Spectra **14**, 41 (2007).
[35]D. Barreca, G. Carraro, and A. Gasparotto, Surf. Sci. Spectra **16**, 1 (2009).
[36]G. Carraro, A. Gasparotto, C. Maccato, D. Peeters, and D. Barreca, Surf. Sci. Spectra **21**, 1 (2014).
[37]M. Inagaki, M. Toyoda, Y. Soneda, and T. Morishita, Carbon **132**, 104 (2018).
[38]F. Le Normand, J. Hommet, T. Szörényi, C. Fuchs, and E. Fogarassy, Phys. Rev. B **64**, 235416 (2001).
[39]J. Zemek, J. Houdkova, P. Jiricek, and T. Kocourek, Langmuir **40**, 19538 (2024).
[40]Z.-H. Sheng, L. Shao, J.-J. Chen, W.-J. Bao, F.-B. Wang, and X.-H. Xia, ACS Nano **5**, 4350 (2011).
[41]I.-Y. Jeon, H.-J. Noh, and J.-B. Baek, Chem. Asian J. **15**, 2282 (2020).
[42]N. Hellgren, M. P. Johansson, E. Broitman, L. Hultman, and J.-E. Sundgren, Phys. Rev. B **59**, 5162 (1999).
[43]M. Benedet, A. Gasparotto, G. A. Rizzi, C. Maccato, D. Mariotti, R. McGlynn, and D. Barreca, Surf. Sci. Spectra **30**, 024018 (2023).
[44]M. Benedet, G. A. Rizzi, A. Gasparotto, L. Zeng, G. Pagot, E. Olsson, V. Di Noto, C. Maccato, and D. Barreca, RSC Adv. **14**, 7221 (2024).
[45]M. Aono, M. Terauchi, Y. K. Sato, K. Morita, T. Inoue, K. Kanda, and K. Yonezawa, Appl. Surf. Sci. **635**, 157677 (2023).
[46]See https://srdata.nist.gov/xps for information about the NIST x-ray photoelectron spectroscopy database.
[47]D. Barreca, A. Gasparotto, C. Maccato, E. Tondello, O. I. Lebedev, and G. Van Tendeloo, Cryst. Growth Des. **9**, 2470 (2009).

SPECTRAL FEATURES TABLE

Spectrum ID #	Element/ Transition	Peak Energy (eV)	Peak Width FWHM (eV)	Peak Area (eV × counts/s)	Sensitivity Factor	Concentration (at. %)	Peak Assignment
01978-02[a]	C 1*s*	284.8	1.8	36 158.4	1.000	32.7	Adventitious contamination and graphitic C atoms in aCN
01978-02[a]	C 1*s*	286.1	1.9	22 076.4	1.000	20.0	C bonded to N atoms in pyrrole- and pyridine-like structural units
01978-02[a]	C 1*s*	287.6	2.5	11 514.9	1.000	10.4	C bonded to "graphitic" N atoms
01978-02[a]	C 1*s*	290.4	3.5	3 593.8	1.000	3.3	Excitation of π-electrons; surface C—OH groups
01978-03[b]	N 1*s*	398.5	1.6	23 874.4	1.676	13.7	Pyridine-type N atoms
01978-03[b]	N 1*s*	399.9	1.8	10 447.9	1.676	6.0	Pyrrole-type N atoms
01978-03[b]	N 1*s*	400.9	1.8	7 913.7	1.676	4.5	"Graphitic" N atoms
01978-03[b]	N 1*s*	403.4	3.0	2 223.0	1.676	1.3	π-electron excitations and "quaternary" nitrogen
01978-04[c]	O 1*s*	530.2	1.8	721.0	2.881	0.3	Cu_xO lattice oxygen
01978-04[c]	O 1*s*	531.8	2.2	12 857.5	2.881	4.7	C—OH groups
01978-04[c]	O 1*s*	533.0	2.3	6 448.8	2.881	2.3	Surface adsorbed water
01978-05[d]	Cu 2*p*	…	…	14 770.1	26.513	0.8	Cu(I) + Cu(II) in Cu_xO
01978-05[e]	Cu $2p_{3/2}$	932.3	1.6	…	…	…	Mostly Cu(I) species in Cu_xO
01978-05[e]	Cu $2p_{1/2}$	952.1	2.0	…	…	…	Mostly Cu(I) species in Cu_xO
01978-06[f]	Cu *LMM*	917.6	…	…	…	…	Mostly Cu(I) species in Cu_xO

[a]The sensitivity factor is referred to the whole C 1*s* signal.
[b]The sensitivity factor is referred to the whole N 1*s* signal.
[c]The sensitivity factor is referred to the whole O 1*s* signal.
[d]The sensitivity factor, peak area, and concentration are referred to the whole Cu 2*p* signal. Copper quantification was made considering the whole Cu 2*p* signal, including shake-up satellites.
[e]The energy is determined at the maximum of the experimental peak.
[f]The KE of the most intense Cu *LMM* feature reported here is used to calculate the copper Auger parameter.

Footnote to Spectrum 01978-01: The wide scan spectrum highlighted the presence of carbon and nitrogen as the most abundant elements along with comparatively lower amounts of oxygen and copper. The N/C atomic percentage ratio, estimated to be ≈0.4, was substantially lower than the value expected for stoichiometric C_3N_4 (1.33), indicating, thus, the occurrence of a C-rich carbon nitride matrix. In line with the spectral features discussed below, Cu signals were consistent with the occurrence of copper oxides, deposited onto aCN following RF-sputtering. The presence of oxygen was ascribed to the presence of Cu_xO species and of surface —OH groups (see **Footnote to Spectrum 01978-04**).

Footnote to Spectrum 01978-02: C 1*s* photoelectron peak was fitted with four contributing bands, whose assignment was performed basing on a detailed literature comparison. The first and most intense one, centered at 284.8 eV, was attributed to graphitic carbon atoms in amorphous carbon nitride (Refs. 30–32), as well as to adventitious surface contamination (Refs. 33–36). The signal at 286.1 eV was mainly ascribed to carbon centers bonded to nitrogen ones in pyrrolic and pyridinic rings of aCN (Refs. 30–32 and 37–39). It is worthwhile noticing that this band includes also contributions from —C≡N and C—NH_x (x = 1, 2) moieties (Refs. 32 and 38), whose presence was confirmed by FT-IR measurements (see above). The component at 287.6 eV was due to C bonded to "graphitic" N atoms, present within the material graphitic network, in place of tri-coordinated C centers (Refs. 31, 32, 37, and 40). Finally, the signal at 290.4 eV was attributed to π-electron excitations, as well as to the concurrent contribution of C—OH groups present on the material surface (Refs. 30 and 33).

Footnote to Spectrum 01978-03: Similarly to the case of C 1*s*, even the N 1*s* signal was fitted with four components. The first one, located at 398.5 eV, was assigned to pyridine-type N atoms (Refs. 4, 30–32, 37, and 41). The band at 399.9 eV was traced back to pyrrole-type nitrogen atoms, as well as to the above discussed —C≡N and —NH_x species (Refs. 4, 30–32, 37, and 41). The third component, at 400.9 eV, was ascribed to graphitic N atoms (Refs. 4, 31, 32, 41, and 42), while the last one, at 403.4 eV, is attributable to π-electron excitations (Refs. 33 and 43). An additional contribution to the 403.4 eV component may arise from "quaternary" N. The latter is essentially the same as graphitic N, except that, at variance with N singly bonded to three carbons and a lone-pair, it releases one electron to form N^+ ions with four valence electrons, which can bond to three carbons in a similar fashion (Ref. 11).

Footnote to Spectrum 01978-04: The O 1*s* photoelectron peak was deconvoluted with three components. The first one, centered at 530.2 eV, was attributed to lattice oxygen from both Cu_2O and CuO (Refs. 34–36 and 44). The main band, centered at 531.8 eV, was assigned to C—OH groups (Refs. 30, 34–36, and 44). The higher energy component, located at 533.0 eV, was attributed to the presence of molecularly adsorbed water on the system surface (Refs. 34–36 and 43–45).

Footnote to Spectra 01978-05 and 01978-06: The Cu 2*p* photoelectron signal displayed two main peaks, with maxima centered at 932.3 eV (Cu $2p_{3/2}$) and 952.1 eV (Cu $2p_{1/2}$), respectively. These signals correspond to the spin–orbit components of Cu(I) oxide (Refs. 33 and 46), the main species in the target nanocomposite. Nevertheless, the two shoulders and the two minor shake-up features at BEs ≈2.4 and ≈9.5 eV higher than the main signals, respectively, are indicative of Cu(II) oxide copresence (Refs. 33–36, 44, and 46), in line with the copper Auger parameter [α = BE(Cu $2p_{3/2}$) + KE(Cu *LMM*) = 1849.9 eV], intermediate between those of Cu_2O and CuO (Refs. 33, 46, and 47).

ANALYZER CALIBRATION TABLE

Spectrum ID #	Element/ Transition	Peak Energy (eV)	Peak Width FWHM (eV)	Peak Area (eV × counts/s)	Sensitivity Factor	Concentration (at. %)	Peak Assignment
…	Au $4f_{7/2}$	84.0	1.1	284 130 5.7	20.735	…	Au(0)
…	Ag $3d_{5/2}$	368.3	0.9	131 620 6.9	22.131	…	Ag(0)
…	Cu $2p_{3/2}$	932.7	1.3	535 062 1.8	26.513	…	Cu(0)

Comment to Analyzer Calibration Table: The peaks were acquired after Ar^+ sputtering with an energy of 3 keV and current of 2.7 μA using ThermoFisher Scientific MAGCIS Dual Beam Ion Source.

GUIDE TO FIGURES

Spectrum (Accession) #	Spectral Region	Voltage Shift (eV)	Multiplier	Baseline	Comment #
01978-01	Survey	0	1	0	…
01978-02	C 1*s*	0	1	0	…
01978-03	N 1*s*	0	1	0	…
01978-04	O 1*s*	0	1	0	…
01978-05	Cu 2*p*	0	1	0	…
01978-06	Cu *LMM*	0	1	0	…

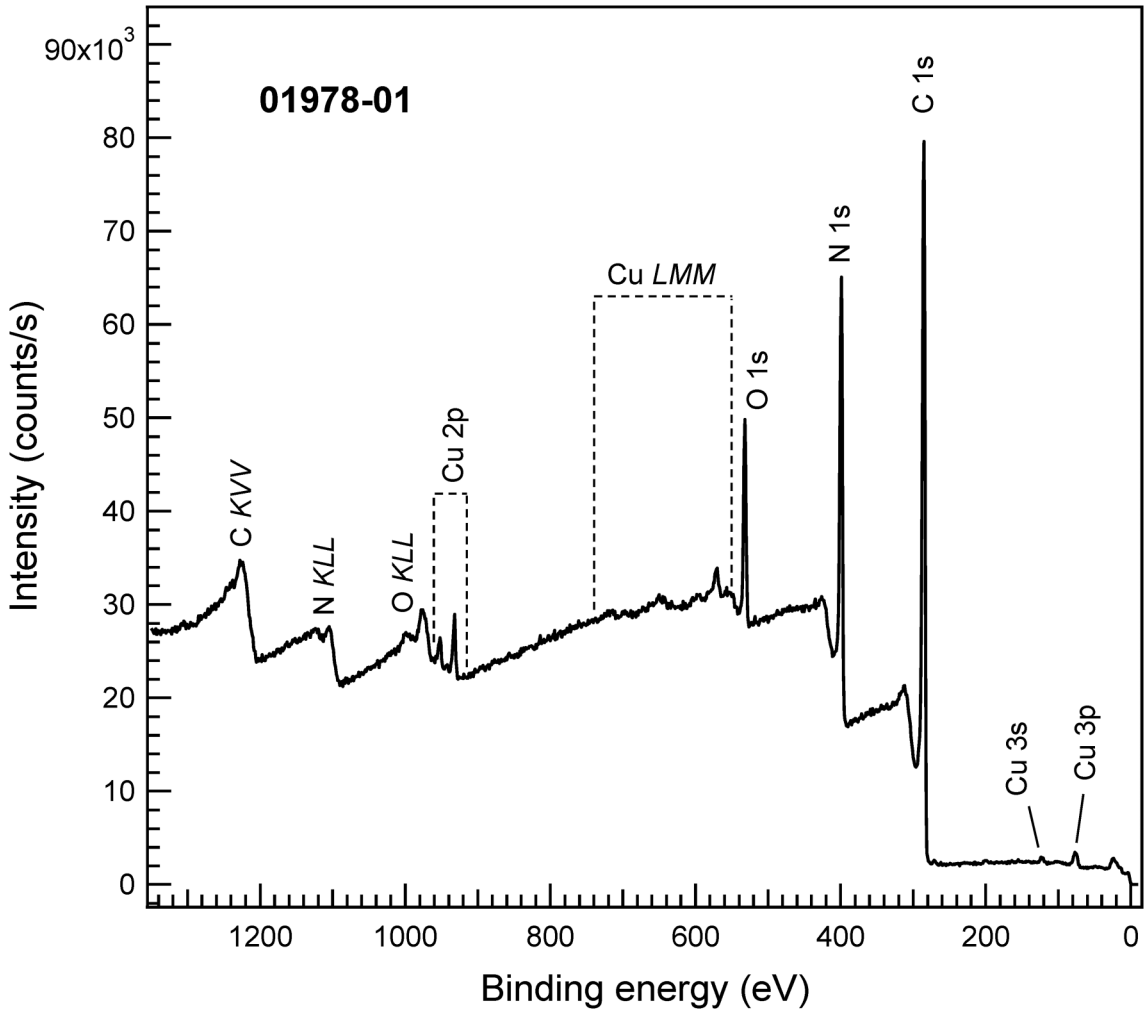

Accession #:	01978-01
■ Specimen:	aCN-Cu_xO
■ Technique:	XPS
■ Spectral Region:	Survey
Instrument:	ThermoFisher Scientific Escalab Xi+
Excitation Source:	Al K_α monochromatic
Source Energy:	1486.6 eV
Source Strength:	200 W
Source Size:	0.5 × 0.5 mm^2
Analyzer Type:	Spherical sector analyzer
Incident Angle:	58°
Emission Angle:	0°
Analyzer Pass Energy:	150 eV
Analyzer Resolution:	1.5 eV
Total Signal Accumulation Time:	612.5 s
Total Elapsed Time:	673.7 s
Number of Scans:	9
Effective Detector Width:	1.5 eV

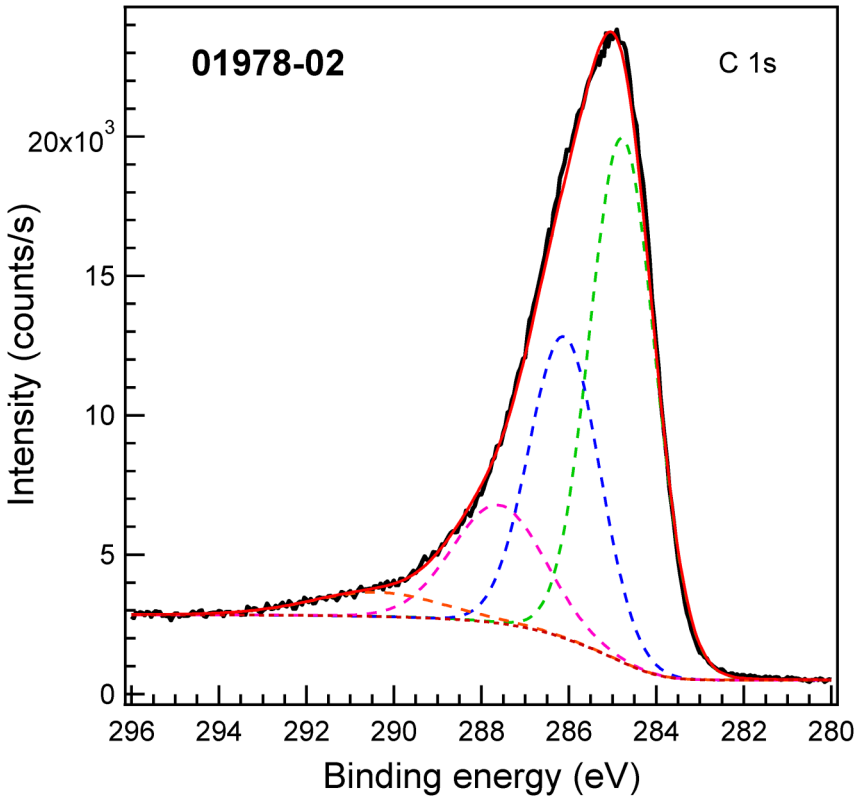

- **Accession #:** 01978-02
- **Specimen:** aCN-Cu_xO
- **Technique:** XPS
- **Spectral Region:** C 1*s*

Instrument: ThermoFisher Scientific Escalab Xi+
Excitation Source: Al K_α monochromatic
Source Energy: 1486.6 eV
Source Strength: 200 W
Source Size: 0.5 × 0.5 mm^2
Analyzer Type: Spherical sector
Incident Angle: 58°
Emission Angle: 0°
Analyzer Pass Energy: 50 eV
Analyzer Resolution: 0.5 eV
Total Signal Accumulation Time: 150.3 s
Total Elapsed Time: 165.3 s
Number of Scans: 6
Effective Detector Width: 0.5 eV

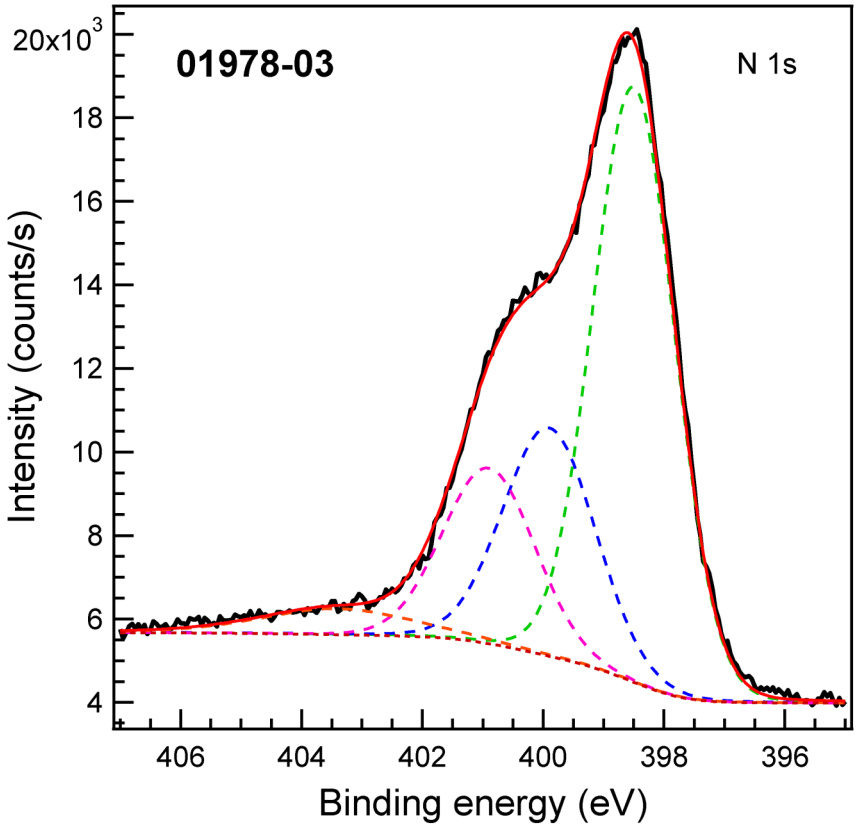

- **Accession #:** 01978-03
- **Specimen:** aCN-Cu_xO
- **Technique:** XPS
- **Spectral Region:** N 1*s*

Instrument: ThermoFisher Scientific Escalab Xi+
Excitation Source: Al K_α monochromatic
Source Energy: 1486.6 eV
Source Strength: 200 W
Source Size: 0.5 × 0.5 mm^2
Analyzer Type: Spherical sector
Incident Angle: 58°
Emission Angle: 0°
Analyzer Pass Energy: 50 eV
Analyzer Resolution: 0.5 eV
Total Signal Accumulation Time: 180.5 s
Total Elapsed Time: 198.6 s
Number of Scans: 10
Effective Detector Width: 0.5 eV

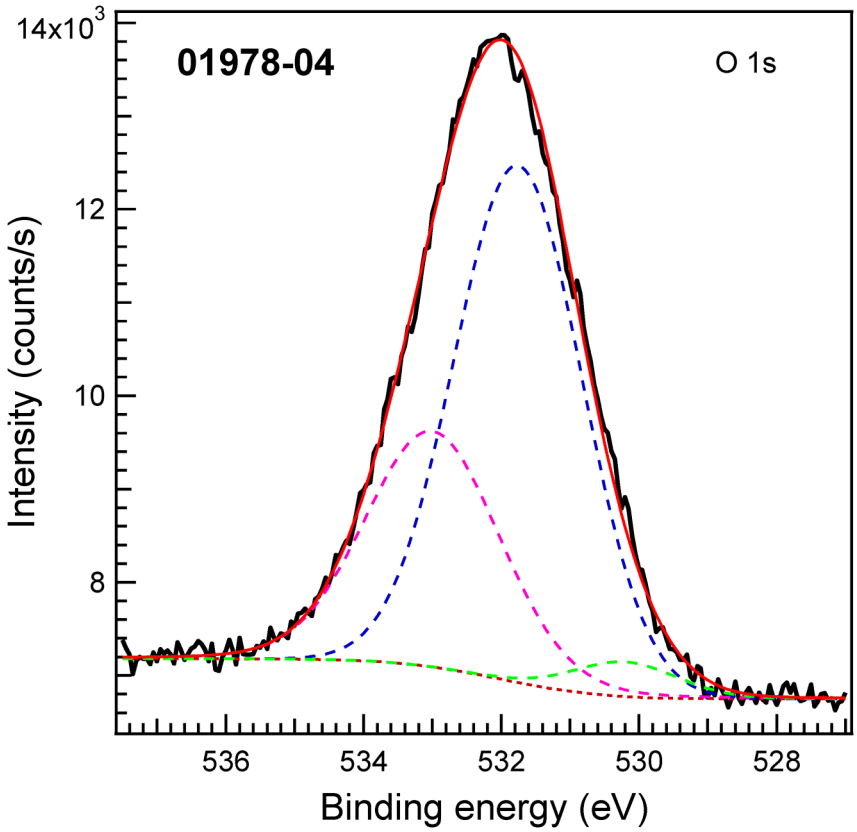

- **Accession #:** 01978-04
- **Specimen:** aCN-Cu_xO
- **Technique:** XPS
- **Spectral Region:** O 1*s*

Instrument: ThermoFisher Scientific Escalab Xi+
Excitation Source: Al K_α monochromatic
Source Energy: 1486.6 eV
Source Strength: 200 W
Source Size: 0.5 × 0.5 mm^2
Analyzer Type: Spherical sector
Incident Angle: 58°
Emission Angle: 0°
Analyzer Pass Energy: 50 eV
Analyzer Resolution: 0.5 eV
Total Signal Accumulation Time: 300.8 s
Total Elapsed Time: 330.8 s
Number of Scans: 15
Effective Detector Width: 0.5 eV

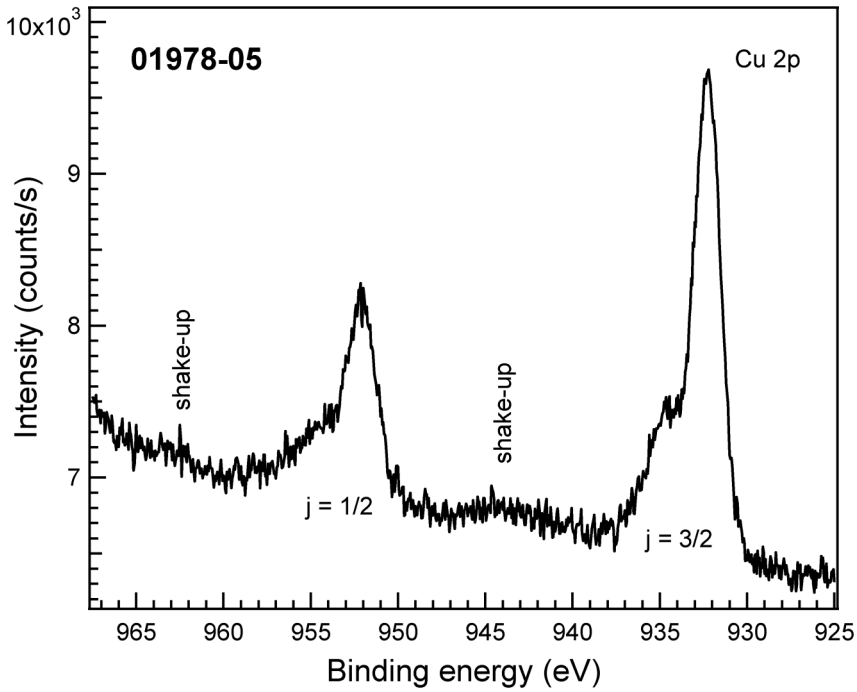

- **Accession #:** 01978-05
- **Specimen:** aCN-Cu_xO
- **Technique:** XPS
- **Spectral Region:** Cu 2*p*

Instrument: ThermoFisher Scientific Escalab Xi+
Excitation Source: Al K_α monochromatic
Source Energy: 1486.6 eV
Source Strength: 200 W
Source Size: 0.5 × 0.5 mm^2
Analyzer Type: Spherical sector
Incident Angle: 58°
Emission Angle: 0°
Analyzer Pass Energy: 50 eV
Analyzer Resolution: 0.5 eV
Total Signal Accumulation Time: 1501.3 s
Total Elapsed Time: 1651.4 s
Number of Scans: 25
Effective Detector Width: 0.5 eV

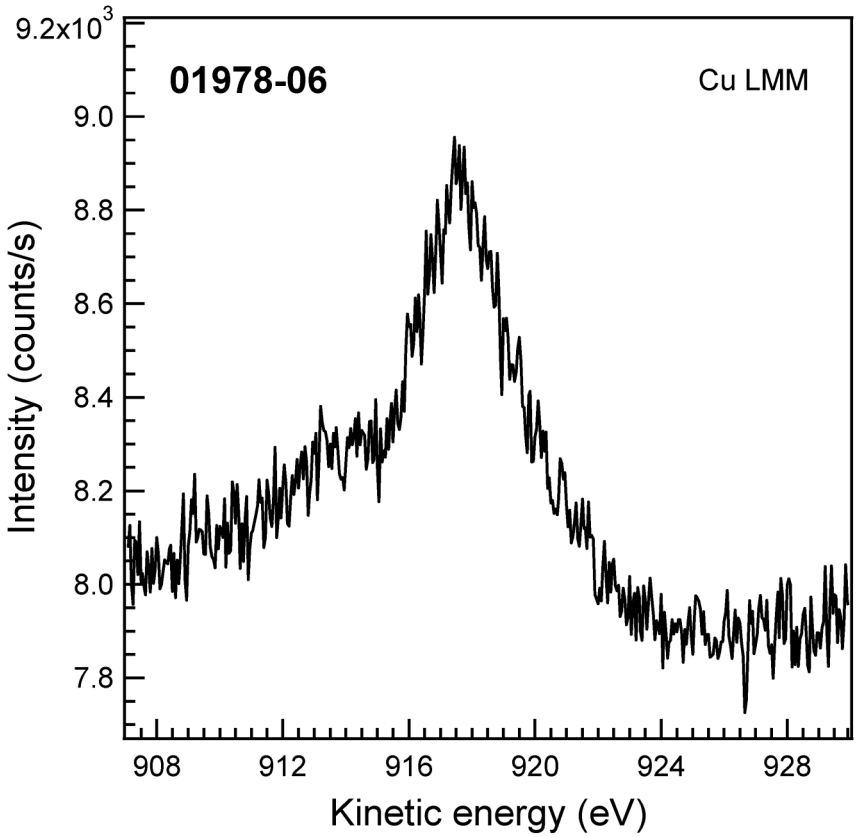

- **Accession #:** 01978-06
- **Specimen:** aCN-Cu_xO
- **Technique:** XAES
- **Spectral Region:** Cu *LMM*

Instrument: ThermoFisher Scientific Escalab Xi+
Excitation Source: Al K_α monochromatic
Source Energy: 1486.6 eV
Source Strength: 200 W
Source Size: 0.5 × 0.5 mm^2
Analyzer Type: Spherical sector
Incident Angle: 58°
Emission Angle: 0°
Analyzer Pass Energy: 50 eV
Analyzer Resolution: 0.5 eV
Total Signal Accumulation Time: 977.0 s
Total Elapsed Time: 1074.6 s
Number of Scans: 39
Effective Detector Width: 0.5 eV